Room Temperature Excitonic Nonlinear Absorption and Refraction in GaAs/AlGaAs Multiple Quantum Well Structures

DANIEL S. CHEMLA, DAVID A. B. MILLER, PETER W. SMITH, FELLOW, IEEE, ARTHUR C. GOSSARD, AND WILLIAM WIEGMANN

Abstract—We present detailed experimental studies and modeling of the nonlinear absorption and refraction of GaAs/AlGaAs multiple quantum well structures (MQWS) in the small signal regime. Nonlinear absorption and degenerate four-wave mixing in the vicinity of the room temperature exciton resonances are observed and analyzed. Spectra of the real and imaginary parts of the nonlinear cross section as a function of wavelength are obtained, and these are in excellent agreement with experimental data. A simple model for excitonic absorption saturation is proposed; it accounts qualitatively for the very low saturation intensities of room temperature excitons in MQWS.

I. INTRODUCTION

THERE has been a recent resurgence of interest in the field of digital optical switching, logic, and nonlinear optical signal processing [1]. In principle, such nonlinear optical elements are attractive for many applications in communications and special-purpose computer systems. In optical communications, the characteristics of large bandwidth, high speed, and the ability to process signals already in the form of light should be particularly useful. For these reasons, nonlinear optical properties of semiconductors have been thoroughly investigated [2]. However, until recently many applications have been impractical because of the lack of suitable materials. Our recent studies of the nonlinear optical properties of excitons in room temperature multiple quantum well structures (MQWS) have demonstrated a new and promising nonlinear material [3]–[6]. In this article, we describe the detailed modeling of this nonlinearity in GaAs/Al$_x$Ga$_{1-x}$As MQWS and show how this information can be used to engineer structures with the desired combination of properties.

The nonlinear optical response of a material is enhanced when the frequencies of the optical fields in interaction are close to or at resonance with a natural frequency of the medium. This is particularly true if the material resonances are sharp, and very efficient nonlinear processes have been observed at the resonances of excitons or exciton complexes in semiconductors [7]. However, in bulk semiconductors excitons can only be observed at low temperature, reducing their interest for practical devices. The observation of exciton resonances at room temperature in the MQWS is therefore very encouraging.

In the last ten years, enormous effort has been devoted to the development of new crystal growth techniques such as molecular beam epitaxy or metal organic chemical vapor deposition. In particular, in the case of the GaAs/Al$_x$Ga$_{1-x}$As system, the recent progress is such that it is now possible to prepare complex structures involving the two compounds with excellent control of the material parameters such as layer thickness, composition, and impurity concentration [8]. This provides new degrees of freedom to "engineer" the band structure of synthetic semiconductor structures with novel electrical and optical properties, as was soon recognized for the superlattices [9]. Quasi-two-dimensional behavior can be produced in structures where a thin layer of low gap semiconductor (e.g., GaAs) is sandwiched between layers of a compound with a larger gap (e.g., Al$_x$Ga$_{1-x}$As), with the electrons and holes generally both confined in the low gap layer [10], [11]. Since the effective masses of the carriers in semiconductors are very small, quantum confinement effects can be seen in layers as thick as several hundred angstroms. In practice, in order to achieve a sufficient optical path several layers are stacked together. Providing that the thickness of the large gap material is large enough to prevent wave function overlap between adjacent wells, the low gap layers act independently. These structures are called multiple quantum well structures; both their electrical and optical properties have been extensively investigated. Excitonic behavior is enhanced because the electron–hole distance is reduced by the confinement [10], [13]–[16]. At low temperatures nonlinear optical processes such as degenerate four-wave mixing (DFWM) [17], resonant Rayleigh scattering [18], and exciton saturation [19] have been observed in MQWS.

Since the average vibrational properties of GaAs and Al$_x$Ga$_{1-x}$As are similar, the temperature broadening of excitons in MQWS should not differ much from that of bulk GaAs. This has led us to contemplate the possibility of observing exciton resonances at room temperature in MQWS and, indeed, it is possible to observe them in these conditions [3], [20]. Exciton resonances at room temperature have been found to saturate quite easily [4] and have very large optical nonlinearities [5], [6]. MQWS have also been shown to exhibit optical bistability [21].

The paper is organized as follows. In Section I, the main properties of the electronic band structure of MQWS are summarized, the linear absorption spectrum is analyzed, and the properties of excitons at room temperature are discussed. In Section II, nonlinear properties of excitons are studied, includ-

ing induced transmission variation and DFWM using two types of light sources (a tunable dye laser and a diode laser). From the nonlinear transmission spectrum and an empirical fit of the linear transmission, we are able to deduce the spectra of both the real and imaginary parts of the nonlinear susceptibility at low intensity, i.e., nonlinear refraction and absorption. The accuracy of these results is tested by comparison to the DFWM spectrum and found to be in excellent agreement with the experimental data. Finally, we discuss the diffusion of photocarriers in MQWS in order to compare our experimental results using picosecond and CW light sources and to present a simple model, based on the screening of the Coulomb interaction by the electron-hole plasma generated through exciton thermal ionization, which accounts qualitatively for our observations.

II. Room Temperature Excitons in Quantum Wells

A recent summary of the band structure of quantum wells in zinc blende structure semiconductors can be found in [22]. For the sake of completeness we restate the main results which are valid for all the semiconductors of this family and we quote the precise values of the parameters for the case of the GaAs/Al$_x$Ga$_{1-x}$As system. The quantization of the electron (e) and hole (h) wave functions in the direction perpendicular to the layers (z), gives rise to discrete energy levels which are labeled by the confinement quantum number $j = 1, 2, 3, \cdots$. As carriers are free to move in the plane of the layers [x, y], two-dimensional subbands are obtained:

$$E_j(\vec{k}) = E_j + \frac{\hbar^2}{2m_\parallel^*}(k_x^2 + k_y^2).$$

In the approximation of infinite well depth, which is fairly accurate for the first few levels, $E_j = (\hbar^2/2m_\perp^*)(j\pi/L_z)^2$ where L_z is the well thickness, as long as this E_j is much less than the well depth. For each subband this corresponds to a step-like density of states

$$g(E) = 0 \qquad E < E_j$$
$$g(E) = m_\parallel^*/\pi\hbar^2 \qquad E \geqslant E_j.$$

The effective mass for the motion parallel to the plane of the layer $m_\parallel^*$ is the same as that for motion perpendicular to the layers $m_\perp^*$ only in the case of electrons (e) ($m^* = 0.067m_0$ for GaAs). For holes the situation is more complicated. The four-fold degeneracy of the upper valence band ($J = 3/2$) is lifted by the confinement giving rise to two hole subbands with $m_\parallel^* \neq m_\perp^*$; the so-called heavy hole (hh) ($m_\perp^* = 0.45m_0$, $m_\parallel^* = 0.1m_0$ for GaAs) and the light hole (lh) ($m_\perp^* = 0.08m_0$, $m_\parallel^* = 0.2m_0$ for GaAs) [15]. Note that at the present time, no good description of the effective masses of the valence bands in quantum wells is available for the motion parallel to the plane of the layers. In the bulk there is only one exciton built up from the electron and the isotopic part of the hole [23]. In quantum wells, for each electron subband the Coulomb interaction produces two excitons involving, respectively, the heavy hole (hh) and the light hole (lh). The optical transition matrix element between valence and conduction subbands is particularly large when the electron and hole wave functions have a large overlap; this occurs when the confinement quantum numbers are the same; $j_e = j_h$. Therefore, the absorption spectrum of a quantum well consists of a series of double steps, one for the hh-e and one for the lh-e transitions with $\Delta j = 0$, both presenting an excitonic structure [10]-[16].

The binding energy of excitons is strongly modified by the confinement. In the case of bulk semiconductors, the binding energy and the Bohr radius are $B_{3D} = -R_y = -e^2\mu^*/2\epsilon^2\hbar^2$ and $a_{3D} = \epsilon\hbar^2/a^2\mu^*$ where μ^* is the proper electron-hole reduced mass taking into account the band structure [23] and ϵ is the dielectric constant. For GaAs, $B_{3D} \sim -4.2$ meV, and $2a_{3D} \sim 300$ Å. The problem of a purely two-dimensional exciton can be solved exactly [24], giving for a "flat" exciton a binding energy $B_{2D} = -4R_y$. The structure of excitons in MQWS depends on four parameters—the well thickness (L_z), the barrier thickness (L_b), and the electron and hole well depths (V_{CB}, V_{VB}). For very wide wells ($L_z > 2a_{3D}$), the exciton structure is hardly affected. For moderately thin layers and substantial well depths, the average electron-hole separation is reduced, resulting in an increased binding energy. However, this is achieved by a shrinkage of the whole charge distribution rather than by a flattening [15]. This is due to the fact that a flattened charge distribution involves a mixture of high-lying states which are not energetically favorable. On the other hand, there is a nonnegligible penetration of the wave functions in the large gap material because V_{CB} and V_{VB} are not infinite. In GaAs this is particularly true for the holes since [10] $V_{CB} \sim 0.85\Delta E_g$ and $V_{VB} \sim 0.15\Delta E_g$ (where ΔE_g is the difference in GaAs and Al$_x$Ga$_{1-x}$As bandgaps) where at room temperature $\Delta E_g \sim 1.247x$ (eV). For very thin layers this penetration becomes important, the carriers are less and less confined, and the exciton structure tends again toward that of a three-dimensional exciton [25]. The binding energy of an exciton in a MQWS is typically maximum in the range $0.5a_{3D} \leqslant L_z < a_{3D}$ for which, in GaAs/Al$_x$Ga$_{1-x}$As MQWS, it peaks between $-2R_y$ and $-3R_y$.

The width of the exciton peak (Γ) in high purity crystals originates from interaction with thermal phonons, and in polar semiconductors it is dominated by LO-phonon broadening. Excitons can be resolved from the continuum if the binding energy is larger than the linewidth; $B > \Gamma$. Usually the binding energy and the Frohlich interaction (which is responsible for the LO-phonon exciton scattering), scale approximately in the same way as a function of the ionicity and the bandgap. Therefore, in bulk semiconductors the condition $B > \Gamma$ is only satisfied at low temperature when the density of thermal LO-phonons is small. In MQWS, when the well thickness is not too small ($L_z \geqslant 50$ Å), the exciton-phonon interaction is hardly modified, so that the LO-phonon contribution to the broadening is expected to remain similar to that of the bulk compound. There is, however, a substantial inhomogeneous broadening which originates from the fluctuations of the confinement energies caused by unavoidable variations of the layer thickness of the order of one monolayer [16], [26]. This is particularly important for thin layers ($\delta E_j/E_j \propto \delta L_z/L_z$).

It appears from this discussion that by choosing the GaAs layer thickness of the order of $L_z \sim 100$ Å and the aluminum content of the order of $x \sim 0.3$, it is possible to increase artificially the binding energy of excitons without large modification of the thermal broadening and to keep the inhomogeneous broadening small enough that the condition $B > \Gamma$ is satisfied at room temperature.

We have reported observation of exciton resonances at room temperature [3], [4] in Sample I (the characteristics of the samples we have studied are given in Table I). The half width

TABLE I
SAMPLE CHARACTERISTICS. ALL THE SAMPLES WE HAVE STUDIED WERE
GROWN BY MOLECULAR BEAM EPITAXY ON GaAs SUBSTRATES. THEY CONSIST
OF N PERIODS OF GaAs LAYERS WITH THICKNESS L_z AND $Al_xGa_{1-x}As$
LAYERS WITH THICKNESS L_b SANDWICHED BETWEEN TWO $Al_xGa_{1-x}As$
LAYERS WITH THICKNESS L_c. (THERE ARE NO CAPS ON SAMPLE I, HOWEVER.)
THE TWO COMPOUNDS ARE UNDOPED WITH RESIDUAL CARRIER
CONCENTRATION $\leq 10^{15} cm^{-3}$ FOR THE GaAs LAYERS AND $\leq 10^{16} cm^{-3}$ FOR THE
$Al_xGa_{1-x}As$ LAYERS.

| Sample	Number of Periods	L_z (Å)	L_b (Å)	x	L_c (Å)
I	77	102	207	.28	0
II	65	96	98	.30	14500
III	84	144	102	.30	3000

Fig. 1. Temperature dependence of the width of the heavy hole–exciton peak for the Sample I. The solid line corresponds to a fit involving a constant contribution describing the inhomogeneous broadening and a contribution proportional to the density of LO-phonons (see text).

at half maximum (Γ) can be measured for the hh exciton on the low energy side of the peak of the absorption spectrum. Fig. 1 shows the measured values of Γ for temperatures varying between liquid helium and room temperature. The solid line represents a fit corresponding to a constant inhomogeneous term Γ_0 plus a term proportional to the density of thermal LO-phonons with proportionality constant Γ_{ph}; i.e.,

$$\Gamma = \Gamma_0 + \Gamma_{ph}/[\exp(\hbar\Omega_{LO}/kT) - 1] \tag{1}$$

where $\hbar\Omega_{LO} = 428$ K $= 36$ meV is appropriate for the GaAs LO-phonon; the fitted value of $\Gamma_0 = 2$ meV is in good agreement with the low temperature luminescence measurements [14], [15]. That of $\Gamma_{ph} = 5.5$ meV is slightly smaller than that of bulk GaAs [27] ($\Gamma_{ph} \sim 7$ meV), confirming that for these layer thicknesses there is no noticeable increase of the LO-phonon–exciton interaction [14]. An example of the room temperature absorption spectrum for Sample II is shown by the crosses in Fig. 2. Not only do the exciton peaks remain visible at room temperature, but we have observed them on this sample up to 70°C. The low energy edge of the absorption spectrum is very abrupt, indeed, too steep to describe the excitons by Lorentzian lineshapes. We have found an excellent empirical fit (Appendix A1) to the room temperature spectrum (solid line) by using Gaussian line shapes for the excitons and a broadened two-dimensional continuum [24] (dashed curves). At $T = 22$°C for this sample, the width of the two excitons is $\Gamma \sim 3$ meV with a separation $\hbar\Omega_l - \hbar\Omega_h \sim 8.5$ meV and a binding energy for the hh exciton of $\hbar\Omega_c - \hbar\Omega_h \sim 10$ meV. The values of the parameters used in the fit are given in Table II.

At room temperature, these excitons are therefore in the very special situation

$$\hbar\Omega_{LO} > kT > B > \Gamma \tag{2}$$

where $\hbar\Omega_{LO} \sim 36$ meV, $kT \sim 25$ meV, $B \sim 10$ meV, and $\Gamma \sim 3$ meV. First of all, because $\hbar\Omega_{LO} > B$, the only possible outcome of a collision of an exciton with an optical phonon is that the exciton is totally ionized into a "free" electron and a "free" hole. From the phonon contribution to the room-temperature width ($\Gamma_p \sim 1.8$ meV) we can evaluate the mean time to thermal ionization by a phonon from the uncertainty principle. Using the form for a Lorentzian line for simplicity, we have the mean time to a collision $\Delta t = \hbar/\Gamma_{ph} \sim 0.4$ ps. Therefore, once an exciton is created by optical absorption, it will live for less than a picosecond before being ionized by an optical phonon.
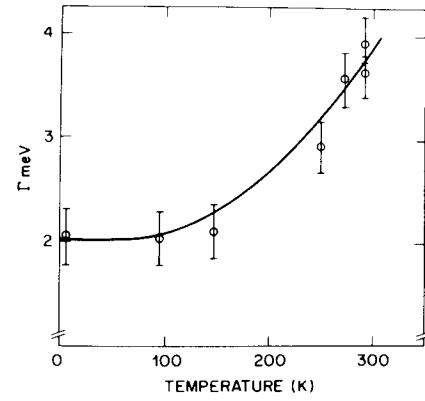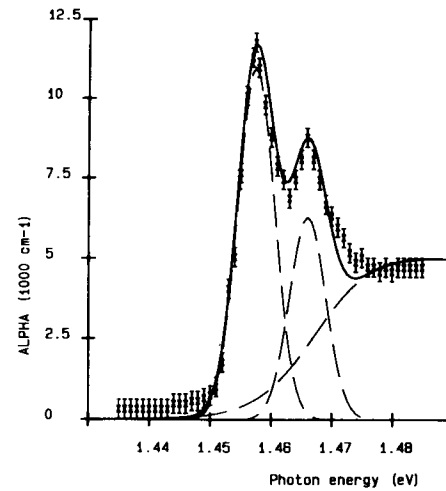

Fig. 2. Absorption coefficient of Sample II near the fundamental absorption edge. The crosses correspond to the experimental data, the solid line is an empirical fit, in which the absorption spectrum is described as the sum of two Gaussian excitons and a broadened two-dimensional continuum (dashed curves).

TABLE II
PARAMETERS USED IN (A1.2) TO OBTAIN THE FIT OF THE ABSORPTION
SPECTRUM OF SAMPLE II, SHOWN BY THE SOLID LINE OF FIG. 2 (h—HEAVY
HOLE, l—LIGHT HOLE, c—CONTINUUM).

j	$\alpha_j (10^3 cm^{-1})$	$\hbar\Omega_j$ (eV)	$\hbar\Gamma$ (meV)
h	11	1.4575	3
l	6.3	1.466	3
c	2.7	1.4675	5

Secondly, because $kT > B$, we expect that relatively few excitons will be reformed from the ionized state, although this needs more detailed justification. If we consider the exciton population at room temperature under steady-state excitation, it is in thermodynamical equilibrium with an electron-hole plasma; $X \rightleftarrows (e + h)$. The electron, hole, and exciton areal densities (i.e., number per unit area) at equilibrium, N_e, N_h, N_X, can be evaluated from the Saha equation of plasma physics adapted to two dimensions, the neutrality condition, and particle conservation (see Appendix A2). The ionization ratio N_e/N_0 and the total carrier concentration per exciton area

$(N_e + N_h)A_X$ calculated in this Appendix are shown in Fig. 3 as a function of N_0, the number of created carrier pairs per unit area. (The carrier pairs will be either excitons or free electrons and holes, depending on whether or not they are ionized.) The ionization ratio is very large. It varies from 1 for small N_0 up to 0.6 for $N_0 \sim 0.5 \times 10^{12}$ cm^{-2} (i.e., 5×10^{17} cm^{-3}), the concentration at which the probability to find one carrier in an exciton area is of the order of 70 percent. Note that our derivation actually underestimates the ionization ratio since it neglects the fact that screening at high densities will reduce the number of possible nonionized exciton states.

We can conclude that, at room temperature, although strong exciton resonances are observed in the absorption spectra, the excitons are almost immediately ionized into a charged plasma of electrons and holes which is particularly effective in screening the Coulomb interaction. This gives to excitons in MQWS the unique nonlinear optical properties discussed in the next section.

III. NONLINEAR OPTICAL PROPERTIES OF GaAs/AlGaAs MQWS AT ROOM TEMPERATURE

Many devices for optical signal processing utilize the variation of the index of refraction n or of the absorption coefficient α induced by an optical excitation. These processes can be described in terms of several parameters; the third-order susceptibility $\chi^{(3)}$; the nonlinear index of refraction n_2 and nonlinear absorption coefficient α_2, or the changes of n and α produced by one electron–hole pair per unit volume; n_{eh} and σ_{eh}. The precise definitions of these parameters as well as their relationships are discussed in Appendix A3. Since we expect the dominant mechanism for exciton nonlinearities in GaAs/AlGaAs MQWS to be the screening of the Coulomb interaction by a charged plasma, we use a time domain description and the parameters n_{eh}, σ_{eh}.

In the usual pump-test configuration shown on the schematic of the experimental setup (Fig. 4) it is possible to measure: 1) the linear absorption coefficient ($I_t = 0$, I_p small), 2) the nonlinear absorption ($I_p \gg I_t \gg \Delta I_t$), and 3) the intensity of the signal beam obtained by diffraction of the pump beam from the amplitude and phase gratings produced by the pump-test interference (i.e., degenerate four-wave mixing). Three lasers were used: a Krypton-laser-pumped oxazine 750 dye laser which could be operated either CW or synchronously mode locked, and two different Hitachi HLP1400 laser diodes. The dye laser is tunable in the 770–870 nm range and when operated mode-locked it delivers a train of pulses with a duration $\delta \sim 6$ ps and a separation $\Delta \sim 12$ ns. One diode laser output consists of a strong mode around 850 nm and a further group of modes around 849 nm. The other laser diode operates at 831 nm. The setup is under computer control and the outputs of the detectors $D1, D2, D3, D4$ can be simultaneously stored after lock-in amplifier processing [15] as the wavelength of the dye laser, the power of the pump, and the test beams or the pulse delay are varied. Samples II and III were studied and presented similar features although the two spectra were displaced by ~ 15 meV owing to the shifts of the band edge associated with the GaAs layer thickness difference.

With the dye laser running mode locked near the hh exciton, we could observe the effects of carrier lifetime on the trans-
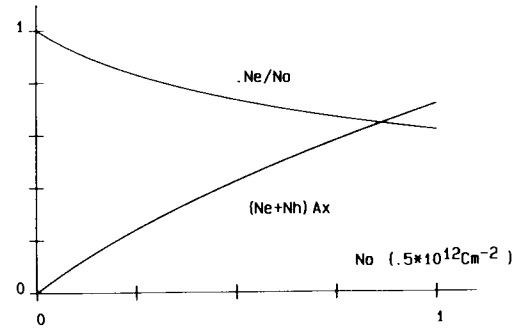

Fig. 3. Thermal ionization ratio N_e/N_0 and combined electron and hole density per exciton area $(N_e+N_h)A_X$ as a function of the number of created carrier pairs per unit area N_0.
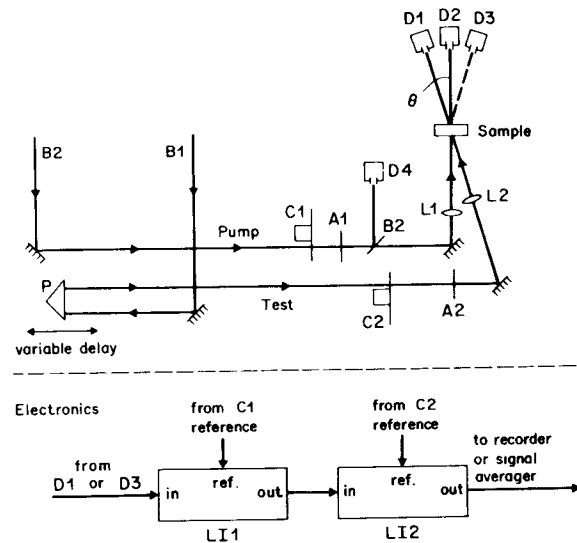

Fig. 4. Schematic of the experimental setup. The laser beams $B1$ and $B2$ originate either from a dye laser or from a diode laser. The test beam can be delayed with respect to the pump beam. Detectors $D1$–$D4$ are silicon photodiodes, choppers $C1$ and $C2$ provide the references for lock-in amplifier signal processing [5]. $A1$ and $A2$ are neutral density filters. Depending on the beam angle θ, one or two lenses are used to focus the beams on the sample.

mission of the test beam as its delay was scanned relative to that of the pump. The test transmission showed the usual step-like rise as the test beam pulse arrival time was adjusted from before to after the pump pulse (with an associated coherence spike). However, it showed no measurable fall over several hundred picoseconds additional delay, indicating that the absorption recovery was much slower than this. The test beam transmission did not, in fact, completely recover between pulses, and the degree to which it recovered its value in the absence of the pump beam was used to estimate the absorption recovery time (and, by assumption, carrier lifetime). Assuming an exponential recovery for simplicity, $\tau = \Delta \log(T_A/T_B)$ where T_A is the change in test transmission for the test pulse arriving just after the pump pulse and T_B is the change for the test pulse just before the pump (i.e., ~ 12 ns after the previous pulse). Using this method in Sample II we found $\tau = 21$ ns for a beam waist radius $w_0 = 25$ μm and $\tau = 31$ ns for $w_0 = 100$ μm. The absorption recovery time is $\tau^{-1} = \tau_R^{-1} + \tau_D^{-1}$ where τ_R is the recombination lifetime and τ_D is the diffusive decay time. In the case of two-dimensional diffusion of a Gaussian distribution which is appropriate for the MQW geometry, $\tau_D = w_0^2/8D$ where D is the diffusion coefficient so that $\tau_R = 32$ ns and

$D = 13$ cm²/s. Assuming that the diffusion is ambipolar and that the hole mobility μ_h is much smaller than that of the electrons, so that $D \sim 2\mathcal{D}_h$, we find that $\mu_h \sim 260$ cm²/V · s in satisfactory agreement with the room temperature high purity material measurements [28].

Fig. 5 shows (a) the linear transmission, (b) the differential nonlinear transmission, and (c) the DFWM spectra obtained on Sample II with the mode-locked laser. The external angle between the pump and the test beam was set to $\theta = 16°$. On the transmission spectrum, the *hh* exciton and *lh* exciton are clearly apparent, and correspond fairly well to the two very contrasted structures of the DFWM spectrum. Conversely, the nonlinear transmission spectrum is very complex with an increase in transmission at the two exciton peaks and a decrease in transmission on each side of the excitons and between them. As a function of the delay between the pump and test pulse, the nonlinear transmission spectrum was found to vary very little for $t = 0$–25 ps. However, significant DFWM was found only in the vicinity of zero pump test delay. This is to be expected as it is only if the pump and test pulses overlap in the sample both spatially and temporally that any grating can be formed. On scanning the delay, we found the half-height width of the DFWM signal to be ~3.1 ps, consistent with the overlap of 6 ps pulses of relatively good coherence.

For our experimental configuration, the diffusive decay time of the grating is

$$\tau_D = (\lambda/4\pi \sin \tfrac{1}{2} \theta)^2 D^{-1} \sim 185 \text{ ps}.$$

Therefore, as discussed in Appendix A3, the DFWM signal is produced by the N_1 carriers generated by one pulse and there is no memory from one pulse to the other. Conversely, the nonlinear transmission is due to all the carriers accumulated before the test pulse N_2 arrives. As a function of N_1 and the pulse separation we have $N_2 = N_1 e^{-t/\tau} [1 - \exp(-\Delta/\tau)]^{-1}$, which does not vary strongly as a function of the delay t (for $\Delta = 12$ ns and $\tau = 21$ ns, $1.3 < N_2/N_1 < 2.3$). For an average pump power in the sample of $P_p = 140$ μW ($I_p \sim 17$ W/cm²) and average test power $P_t = 35$ μW, the DFWM efficiency (i.e., the reflection efficiency of the test beam into the signal beam) at the maximum is $\rho_s \sim 0.44 \times 10^{-4}$ and the relative change of transmission is $\rho_t \sim 10^{-2}$, all these values being corrected for reflection losses. The quadratic dependence $\rho_s \propto I_p^2$ was verified at the peak of the DFWM spectrum up to $P_p = 500$ μW: above this value apparently the onset of saturation reduces the efficiency. As shown in Appendix A3, the microscopic quantity measured in the DFWM experiment is $\sigma = 1/2 |2\pi/\lambda \, n_{eh} + (i/2)\sigma_{eh}|$. For these measurements

$$\sigma \sim (2.8 \pm 1.4) \times 10^{-14} \text{ cm}^2. \tag{3}$$

In order to interpret the nonlinear transmission spectrum we have used the following procedure. As discussed in Appendix A1 the absorption coefficient spectrum $\alpha(\hbar\omega)$ is well described by the analytical formula (A1.2) and a set of nine parameters $Z = \alpha_h, \Omega_h, \Gamma_h \cdots$. In the small signal regime they are expected to depend linearly on the carrier density and, therefore, for a constant pump intensity, also linearly on the absorption coefficient $\alpha(\hbar\omega)$. If we assume that at the frequency of maximum absorption α_M the pump-induced photocarriers produce a change ΔZ_M in a given parameter, then at the photon energy

$\hbar\omega$ the same pump intensity produces a change $\Delta Z(\hbar\omega) = \Delta Z_M \alpha(\hbar\omega)/\alpha_M$. At each frequency the change of absorption can be calculated from (A1.2) evaluated for the parameters Z and $Z + \Delta Z(\hbar\omega)$ and compared to the experimental spectra. It was surprisingly easy to find the excellent fit shown in Fig. 6 where the crosses correspond to the spectra of Fig. 5(b) corrected for the small variation of the laser intensity as its wavelength is tuned, and the solid line corresponds to the set of parameter variations ΔZ_M given in Table III. The fit was easy to perform because 1) the effects of the variations of the exciton parameters were found to be almost independent for the *hh* exciton and the *lh* exciton and 2) the continuum parameters remained unchanged. This shows that at the power at which the experiments were performed the excitons are affected, but saturation of interband transitions is not yet reached. The two excitons experience a loss of absorption at the peak of the order of 5 percent, which is accompanied, for the *hh* exciton, by a broadening such that the area of the peak remains fairly constant. Both excitons experience a very small shift, which is, however, important in obtaining a good fit. Note that although our empirical fit does not represent a model, it indicates that the effect of the pump is directly proportional to the number of carriers it generates. Other attempts (for instance ΔZ independent of $\hbar\omega$) failed to reproduce the experimental data.

The refractive index and the absorption coefficient are related by the Kramers-Kronig relations [29], which remain valid for a material containing a fixed number of carriers (for in-
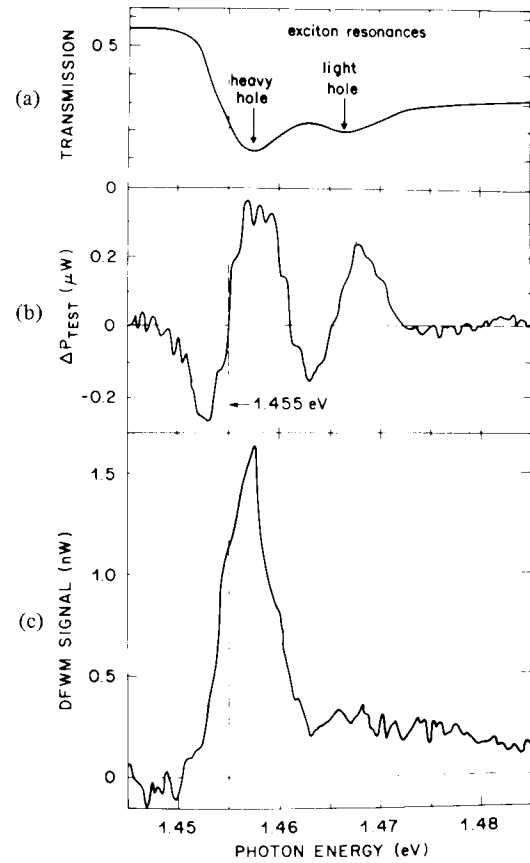

Fig. 5. Experimental spectra of (a) the transmission of the sample, (b) the differential nonlinear transmission induced by the pump on the test beam, and (c) the intensity of the degenerate four-wave mixing signal.
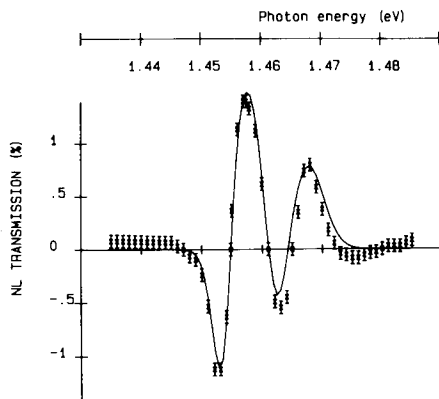
Fig. 6. Fit of the experimental differential spectrum of Fig. 5 as discussed in the text (crosses are experimental points).

TABLE III
VARIATION OF THE PARAMETERS LISTED IN TABLE II WHICH GIVE THE BEST FIT FOR THE NONLINEAR TRANSMISSION SPECTRUM OF SAMPLE II.
[FIGS. 5(b) AND 6.]

j	$\Delta\alpha_j/\alpha_j$	$\Delta(\hbar\Omega_j)$	$\Delta(\hbar\Gamma_j)$
h	-5.8×10^{-2}	-5×10^{-5}	2×10^{-4}
l	-4.8×10^{-2}	-5×10^{-5}	0
c	0	0	0

Fig. 7. Real part (n_{eh}) and imaginary part (σ_{eh}) of the nonlinear cross section of Sample II. σ_{eh} is derived directly from the fit of the differential spectrum shown in Fig. 6 and Table III; n_{eh} is calculated from the same fit using the Kramers–Kronig relations.

stance doped material). The absorption coefficient and the refractive index of a semiconductor containing a *fixed* number of photocarriers are therefore also related by the Kramers–Kronig relations. The changes of refractive index associated with the change of absorption coefficient is

$$\Delta n(\omega) = \frac{c}{\pi} P \int_0^\infty \frac{\Delta\alpha(\omega')d\omega'}{\omega'^2 - \omega^2} \tag{4}$$

where the symbol P indicates that the principal value of the integral has to be evaluated. Since empirically interband transitions do not contribute to $\Delta\alpha$, this quantity involves only Gaussian functions and Δn is directly related to the plasma dispersion function on which an abundant numerical analysis literature exists; this helps in providing an accurate integration of (4). The results of this calculation using the fit of the nonlinear transmission and expressed in terms of the convenient parameters $\sigma_{eh}(\omega)$ and $n_{eh}(\omega)$ are shown in Fig. 7.

A severe test of the accuracy of the $\sigma_{eh}(\omega)$ and $n_{eh}(\omega)$ spectra is that they should reproduce the experimental DFWM spectra. We have checked this in the following way; from $\sigma_{eh}(\omega)$ and $n_{eh}(\omega)$ we calculate the *absolute changes* of absorption and refractive index for the pump laser intensity $\Delta\alpha(\omega)$ and $\Delta n(\omega)$, then according to the analysis of Appendix A2 the DFWM spectrum is given by

$$\rho_s(\omega) = K\left[\left(\frac{2\pi}{\lambda}\Delta n(\omega)\right)^2 + \left(\frac{1}{2}\Delta\alpha(\omega)\right)^2\right] l_\alpha^2 e^{-\alpha l} \tag{5}$$

where the constant K accounts for the effective number of carriers which contribute to DFWM as compared to those which contribute to the nonlinear transmission, i.e., $K \propto (N_1/N_2)^2$. The excellent agreement with the experimental spectrum shown
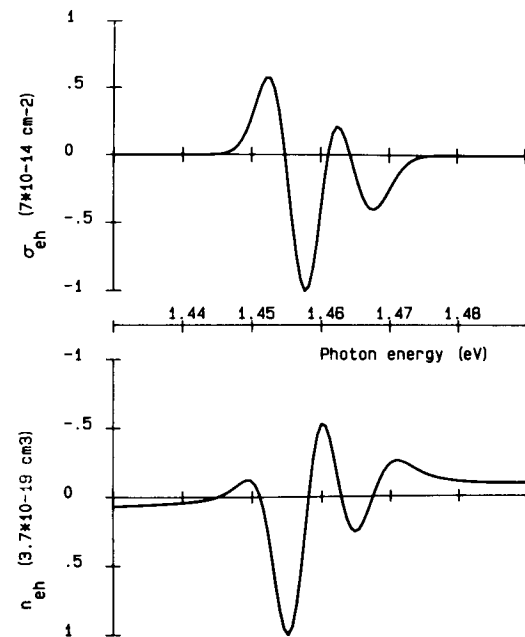
in Fig. 8 is obtained for $N_1/N_2 = 0.3$ whereas the values of τ and Δ give $N_1/N_2 = 0.43$. This difference is well within the accuracy of our measurements. Let us note that the value of N_1/N_2 only affects the amplitude of the predicted DFWM spectra which can be reduced by a number of factors. However, the most important conclusion of this analysis is the fact that the highly structured $\sigma_{eh}(\omega)$ and $n_{eh}(\omega)$ very accurately describe the shape of the experimental DFWM spectrum. This is an indication that they represent pretty well the actual behavior and can be used to evaluate operating characteristics of devices, such as optical bistable devices, based on MQW samples. The maximum values of the nonlinearities are very large; $\sigma_{eh} \sim 7 \times 10^{-14}$ cm^{-2} ($\alpha_2 \sim 39$ cm/W) or $n_{eh} \sim 3.7 \times 10^{-19}$ cm^3 ($n_2 \sim 2 \times 10^{-4}$ cm^2/W) corresponding to $|\chi^{(3)}| \sim 6 \times 10^{-2}$ ESU, that is, about 10^6 times the $\chi^{(3)}$ of silicon at room temperature.

Indeed, these figures are so large that nonlinear optical effects can be observed with CW laser diodes. The simplest process involving a diode which can be investigated is a nonlinear transmission induced by a pump beam from a laser diode operating at a fixed wavelength (in this case 831 nm) on a tunable test beam from a dye laser. Then, as long as $P_p \gg P_t$, the number of photocarriers is approximately constant as the test beam wavelength is tuned. This experiment complements the previous nonlinear absorption measurements where the pump beam and test beam were at the same wavelength. Examples of the change of transmission and of a differential spectrum of the nonlinear transmission are shown in Figs. 9 and 10. The two spectra of Fig. 9 were obtained for $P_p = 0$ and $P_p \sim 5$ mW whereas the differential spectrum of Fig. 10 was obtained for $P_p \sim 290$ μW, $P_t \sim 38$ μW; in both cases, the spot radius was $w_0 \sim 20$ μm. For the differential spectrum the number of photocarriers was $N \sim 1.6 \times 10^{16}$ cm^{-3} and the maximum change of absorption coefficient was $\Delta\alpha \sim 10^3$ cm^{-1}. The
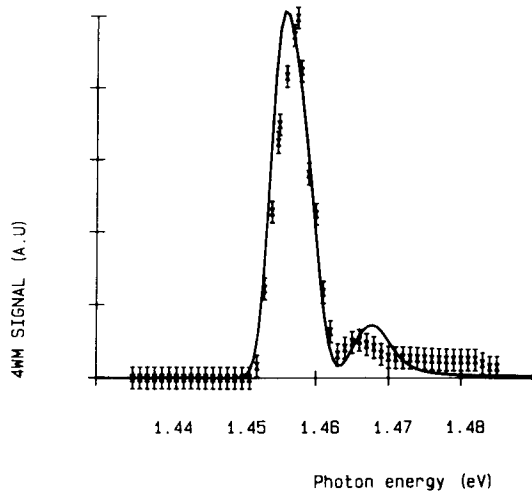
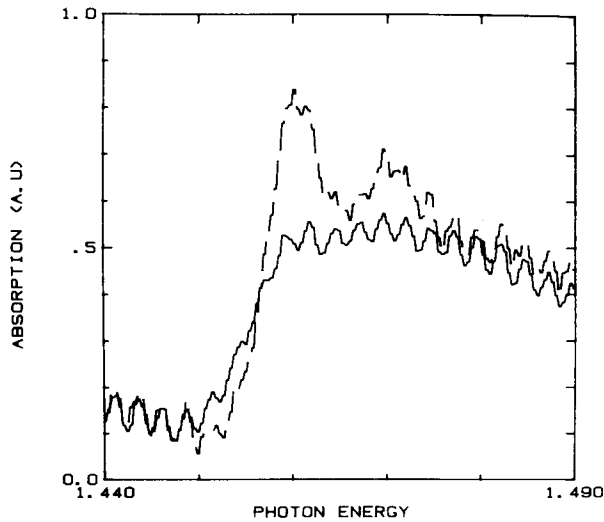Fig. 8. Comparison of the experimental DFWM spectrum to the prediction of our model.

Fig. 9. Spectra measured with a dye laser test beam at very low power, with (solid line) and without (dashed line) a ~5 mW pumping beam at 831 nm from a diode laser. Spot diameter ~40 μm. (The fast ripples in these spectra are Fabry–Perot fringes in a thin glass plate covering the sample.)

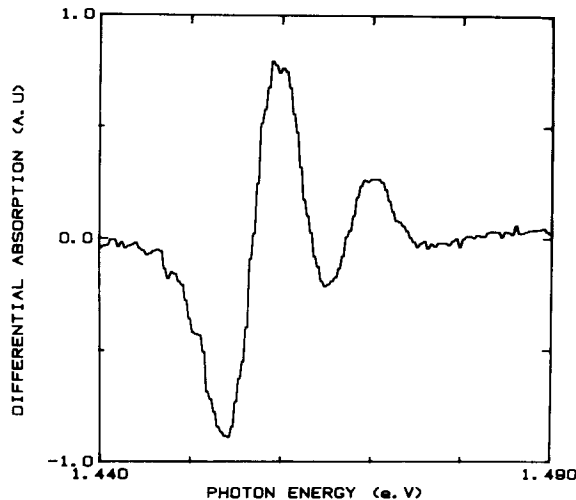
Fig. 10. Change in test beam transmission due to the 831 nm diode pump excitation with 290 μW of diode power.

curve of Fig. 9 can be fitted with the procedure described above and constant parameter variations (ΔZ independent of $\hbar\omega$). Again, the continuum contribution does not change and the exciton parameter variations giving the best fit are in good agreement with those of Table III. This provides an important confirmation of our model of the nonlinear absorption process because it demonstrates directly that the change in absorption is the same regardless of whether the material is excited at the exciton resonances or at some completely different energy. This is what would be expected from our proposal that even when excitons are created directly they ionize rapidly and the change of absorption results from screening by free carriers. The absolute change of absorption coefficient at the hh exciton peak was measured as a function of the pump power up to $P_p \sim 5$ mW. It was found to vary linearly up to $P_p \sim 1.7$ mW ($I_p \sim 270$ W/cm^2) and then to saturate.

Finally, a DFWM experiment was performed using the diode laser output as the sole light source [6]. The external beam angle was set to ~1.5° to increase the grating lifetime to $\tau_G \sim 12.5$ ns. In order to match the absorption of the Sample II to the diode wavelength (in this case ~851 nm) the sample was cooled to $T \sim 14.7$°C (the temperature at which the measurements were made), although the DFWM signal was observable between 6 and 22°C. The quadratic dependence of the DFWM signal was verified from $P_p = 100$ μW to 2.4 mW. Above this value the onset of the saturation reduces the efficiency [6]. For a pump intensity $I_p \sim 17$ W/cm^2, the conversion efficiency is $\rho_3 \sim 0.55 \times 10^{-4}$; both of these values have been corrected for reflection. In this experiment the effective number of carriers which contribute to the DFWM is $N_{eff} \sim 10^{16}$ cm^3 (Appendix A3). Because the laser output consists of several modes we measure an average of σ, i.e., $\langle\sigma\rangle \sim (3.6 \pm 1.8) \times 10^{-14}$ cm^2 in very good agreement with the result of the experiment with the mode locked dye laser, and thus confirming the extremely large nonlinearities of room temperature excitons in MQWS.

The correct description of Coulomb interaction screening in semiconductors requires the use of many body theory and is beyond the scope of this article. However, it is possible to develop a simple model which qualitatively describes the main features of exciton saturation at room temperature in a two-dimensional geometry. Saturation originates either from the exhaustion of the number of available states or from the Coulomb interaction screening by the electron–hole plasma generated directly or through thermal ionization. The exciton wave function is built up from states of the Brillouin zone such that $|k| \lesssim 1/a_X$ where a_X is the exciton radius (which in a quantum well is different from the bulk Bohr radius a_{3D}). This is equivalent to saying that a density N_X of excitons causes a relative decrease of the available states ~$(1 - N_X A_X)$ where $A_X = \pi a_X^2$ is the exciton area. The screening of a point charge in a two-dimensional electron–hole gas has been discussed at length [30], [34]. The case of multiple layer systems is intermediate between two- and three-dimensional systems because the electrostatic interaction between layers is not negligible, and a screened potential falls off rapidly at a distance above the Bohr radius. We approximate this situation by the following crude model. We assume that a point charge acts as a point defect which

perturbs the semiconductor locally sufficiently so that excitons cannot be created within some distance of it [35]. A good evaluation of the size of the perturbed region is again the exciton area. In the low concentration limit the point defects act independently so that Poisson statistics apply. As shown in Appendix A2, they induce a relative change of absorption $\sim \exp\left[-(N_e + N_h)A_X\right]$. The total relative decrease of absorption due to the equilibrium between N_X excitons, N_e electrons, and N_h holes is

$$\frac{\alpha(I)}{\alpha_0} \simeq (1 - N_X A_X) \exp\left[-(N_e + N_h)A_X\right] \quad (6)$$

where N_X, N_e, and N_h are implicit functions of $\alpha(I)$. The evaluation of (6) is analyzed in Appendix A2; in the small signal regime it reduces to the simple saturation form

$$\frac{\alpha(I)}{\alpha_0} \simeq \frac{1}{1 + \left(\dfrac{2\tau\alpha_{Ga}L_z A_X}{\hbar\omega}\right)I} \quad (7)$$

where α_{Ga} is the material linear absorption coefficient when only the GaAs layer thickness is considered (see Appendix A2).

The "saturation intensity" $I_s = (1/\alpha_{Ga}L_z)(\hbar\omega/2\tau A_X)$ has a simple physical interpretation. $\Delta I = \hbar\omega/2\tau A_X$ is the intensity which should be absorbed in one exciton area to generate either an electron or a hole per life time, and $I_s = \Delta I/\alpha_{Ga}L_z$ is the intensity which must be incident on the layer in order for ΔI to be absorbed. For $L_z \sim 100$ Å, Miller et al. [11] have obtained a binding energy $B \sim 9$ meV from which we can deduce $a_X \sim 65$ Å so that application of (7) to Samples I and II gives, respectively, $I_s \sim 490$ W/cm^2 and $I_s \sim 190$ W/cm^2. For such a simple model these values compare quite well to $I_s = 580$ W/cm^2 for Sample I [5] and $I_s = 300$ W/cm^2 for Sample II (derived from the approximate relationship $\alpha_2 \sim \alpha/I_s$). Although a more sophisticated theory might give a better description of the exciton saturation, the quantitative agreement of our crude approach with experiment indicates that it correctly accounts for the dominant mechanisms. However, it is not sophisticated enough to explain why the nonlinear spectra take on the particular shape they do.

IV. CONCLUSION

We have shown that by a proper design of multiple quantum well structures it is possible to observe excitonic absorption peaks at room temperature. In these unusual conditions, excitons created by optical absorption transform rapidly by thermal ionization into an electron–hole plasma with very effective screening properties. The conjunction of these two mechanisms gives to MQWS exceptional nonlinear optical properties. In the small signal regime we have investigated optical nonlinearities by nonlinear absorption and degenerate four-wave mixing measurements, from which we have been able to obtain the spectral dependence of the absorptive and refractive contributions. By performing the first degenerate four-wave mixing experiment with a commercial laser diode as the sole light source, we have proved experimentally that the nonlinearities of MQWS can be utilized in the actual conditions of operation of optical communication systems. Finally, we have proposed a simple model which quantitatively describes the saturation characteristics of room temperature excitons in MQWS.

These results give us the design parameters to engineer the nonlinear optical properties of GaAs/AlGaAs MQWS for specific applications. This material should be considered as only the first of many. The development of the growth techniques and the new degrees of freedom recently revealed by the successful fabrication of strained superlattices and preparation of MQWS with quaternary semiconductor compounds should result in promising new structures and new conditions of operation.

APPENDIX A1
ANALYTICAL EXPRESSION FOR THE ABSORPTION COEFFICIENT CLOSE TO THE BAND EDGE

In a perfect crystal and at $T = 0$ K the absorption spectrum consists of infinitely narrow lines at the exciton energies and a continuum above the band edge. The Coulomb interaction causes an enhancement of the absorption even above the band edge where the excitons are ionized. This effect is described by the so-called Sommerfeld factors which, in the case of a two-dimensional density of state, can be written [24]

$$F(\hbar\omega) = \frac{2}{1 + \exp\left\{-2\pi\left[(\hbar\Omega_c - \hbar\omega)/R_y\right]^{-1/2}\right\}} \quad (A1.1)$$

where $\hbar\Omega_c$ is the energy of the continuum edge and R_y is the Rydberg constant of the material $R_y = e^2\mu^*/2\epsilon^2\hbar^2$.

To describe the absorption by the two excitons (lh-e, hh-e) and the continuum at room temperature and therefore to account phenomenologically for the temperature and crystal imperfection broadenings we have used the following expression:

$$\alpha(\hbar\omega) = \alpha_h \exp\left[-\frac{(\hbar\omega - \hbar\Omega_h)^2}{2(\hbar\Gamma_h)^2}\right] + \alpha_l \exp\left[-\frac{(\hbar\omega - \hbar\Omega_l)^2}{2(\hbar\Gamma_l)^2}\right]$$

$$+ \frac{\alpha_c}{1 + \exp\left(\dfrac{\hbar\Omega_c - \hbar\omega}{\hbar\Gamma_c}\right)}$$

$$\times \frac{2}{1 + \exp\left\{-2\pi\left[|\hbar\Omega_c - \hbar\omega|/R_y\right]^{-1/2}\right\}}. \quad (A1.2)$$

We have not attempted to include separately the two different continuum contributions from the lh and hh subbands. The fit of Fig. 2 corresponds to the values of the parameters listed in Table II. Note that this is a semiempirical fit from which one should avoid extracting too precise conclusions, such as, for example, the exact position of the continuum.

APPENDIX A2
MODEL FOR SATURATION OF EXCITON ABSORPTION

We assume that the exciton, electrons, and holes are in a thermodynamic equilibrium

$$X \rightleftarrows (e + h)$$

analogous to that of a high temperature hydrogen plasma. It is well known in plasma physics that in three dimensions the concentrations of particles are related by the Saha equation $N_e N_h/N_X = 2(m_e kT/2\pi\hbar^2)^{3/2} \exp(-R_y/kT)$. To transform this equation to two dimensions we use the proper density of states $g(E) = m_e^*/\pi\hbar^2$ and areal particle densities so that

$$\frac{N_e N_h}{N_X} = \frac{m_e^*}{\pi\hbar^2} kT \exp\left(\frac{-B}{kT}\right) \quad (A2.1)$$

where B is the binding energy of the two-dimensional exciton.

The absorption coefficient of the GaAs layers is $\alpha_{Ga} = \alpha(L_z + L_b)/L_z$ and the number of photons absorbed per exciton lifetime in one layer is $N_0 = \tau L_z \alpha_{Ga} I/\hbar\omega$. The particle conservation and neutrality conditions are written, respectively,

$$N_0 = N_X + N_h \qquad (A2.2a)$$

$$N_e = N_h. \qquad (A2.2b)$$

Let us consider a sample of area A containing one exciton of area A_X. If there is one point charge in the sample the probability not to find it within the exciton is $P_1 = 1 - A_X/A$; if there are $\mathfrak{N}$ charges acting independently the probability that none of them is within the exciton is $P = (1 - A_X/A)^{\mathfrak{N}}$. Let $N_e + N_h = \mathfrak{N}/A$ be the total charge density. Then for large $(N_e + N_h)$

$$P = [1 - (N_e + N_h)A_X/(N_e + N_h)A]^{(N_e + N_h)A}$$
$$\rightarrow \exp[(-N_e + N_h)A_X].$$

Since an area density N_X of excitons fills a fraction $\sim N_X A_X$ of all possible exciton states, the relative reduction of absorption when N_X excitons are in equilibrium with N_e electrons and N_h holes is

$$\bar{\alpha} = \frac{\alpha(I)}{\alpha_0} = (1 - N_X A_X) \exp[-(N_e + N_h)A_X]. \qquad (A2.3)$$

To evaluate this equation let us introduce two auxiliary variables: $v = A_X(m_e^*/\pi\hbar^2)kT \exp(-B/kT)$ is a pure number and $I_s = \hbar\omega/2L_z \alpha_{Ga}\tau A_X$ giving

$$\bar{\alpha} = \left(1 - \frac{\bar{\alpha}I}{2I_s} + \frac{v}{2}\right) \left[\left(1 + \frac{2\bar{\alpha}I}{vI_s}\right)^{1/2} - 1\right]$$
$$\cdot \exp\left[\left(-v\left(1 + \frac{2\bar{\alpha}I}{vI_s}\right)^{1/2} - 1\right)\right].$$

In the limit $I \rightarrow 0$ this reduces to

$$\alpha(I) = \frac{\alpha_0}{1 + I/I_s}. \qquad (A2.4)$$

APPENDIX A3
THIRD-ORDER NONLINEAR PROCESSES: TIME AND FREQUENCY DOMAIN DESCRIPTION

Third-order nonlinear processes related to photocarriers can be described in terms of different parameters; the third-order susceptibility $\chi^{(3)}$; the nonlinear refractive index and absorption coefficient n_2, α_2; and the change of refractive index or absorption coefficient per electron–hole pair per unit volume n_{eh}, σ_{eh}. In this Appendix the three descriptions are related and the formulas used to analyze our experimental data are derived.

Let us first consider the time domain description. If an intensity $I(t)$ is incident on the sample the absorbed intensity is $I_A(t) = T\alpha l_\alpha I(t)$ where T is the transmission coefficient at the air–sample interface and $l_\alpha = \int_0^l e^{-\alpha z} dz = (1 - e^{-\alpha l})/\alpha$ is the effective interaction length taking into account the absorption, l being the sample thickness. The carrier density is

$$N(t) = \frac{l_\alpha}{l} \frac{\alpha}{\hbar\omega} \int_{-\infty}^{t} I(t') \exp[-(t - t')/\tau] \, dt' \qquad (A3.1)$$

where the decay time τ depends both on the recombination lifetime τ_R and the diffusive decay time τ_D; $\tau^{-1} = \tau_R^{-1} + \tau_D^{-1}$. For a sinusoidal intensity modulation with spatial frequency Λ (appropriate in DFWM), $I_G \propto \cos(2\pi x/\Lambda)$, the diffusive decay time is $\tau_D = \Lambda^2/4\pi D$ whereas for a Gaussian distribution (appropriate for nonlinear absorption), $I_A \propto \exp[-2(x^2 + y^2)/W_0^2]$ and a two-dimensional diffusion in the $[x, y]$ plane, $\tau_D \sim W_0^2/8D$. In the case of ambipolar diffusion $D = 2D_e D_h/(D_e + D_h)$.

Accordingly, we introduce two decay times $\tau_A^{-1} = \tau_R^{-1} + 8D/W_0^2$ and $\tau_G^{-1} = \tau_R^{-1} + 4\pi D/\Lambda^2$. Two configurations are of interest: 1) excitation by a CW laser and 2) excitation by a train of pulses short compared to the lifetime and separated by a time Δ.

In case 1) the relevant number of carriers, $N_A = T(l_\alpha/l)(\alpha\tau_A/\hbar\omega)I$ or $N_G = T(l_\alpha/l)(\alpha\tau_G/\hbar\omega)I$, is the number of carriers accumulated in one decay time. In case 2) the number of carriers generated by one pulse is $N_1 = T(l_\alpha/l)(\alpha J/\hbar\omega)$ where J is the energy fluence per pulse. The relevant number of carriers is $N_{A,G}(t) = N_1 e^{-t/\tau}[1 - \exp(-\Delta/\tau)]^{-1}$ with $\tau = \tau_A$ or τ_G according to the geometry of the excitation. Note that for $\Delta \gg \tau$, $N(0) \sim N_1$. A schematic of the variation of $N_{A,G}(t)$ for $\Delta \sim \tau_A \gg \tau_G$ is shown in Fig. 11.

The nonlinear absorption does not depend on the relative phase of the pump and the test fields and all photocarriers participate in the process. For $I_p \gg I_t$, the transmission of the sample at $t = 0$ is (allowing for two surface reflections) $\rho_t = I_t(l, I_p)/I_t(0) = T^2 \exp(-(\alpha + \Delta\alpha)l)$ with $\Delta\alpha = \sigma_{eh} N_p$ and

$$\rho_t \sim T^2 [1 - \sigma_{eh} N_A(t)l] e^{-\alpha l} \qquad (A3.2a)$$

$$\rho_t \sim T^2 [1 - \sigma_{eh} N_A l] e^{-\alpha l} \qquad (A3.2b)$$

respectively, for a short pulse and a CW excitation with $\Delta\alpha \ll \alpha$.

The DFWM is sensitive to the relative phase of the pump and test fields, so that only the photocarriers coherently generated by the pump test interference are effective. The relevant lifetime is the grating lifetime τ_G and the diffraction efficiency is [36]

$$\rho_s = \frac{I_s(l)}{I_t(0)} = \left| J_1 \left[\left(\frac{2\pi n_{eh}}{\lambda} + i \frac{\sigma_{eh}}{2} \right) N_G l \right] \right|^2 e^{-(\alpha + \Delta\alpha)l} \qquad (A3.3)$$

where $J_1(x)$ is the first order Bessel function. In the small signal regime for which $J(x) \rightarrow (1/2)x$ a natural parameter appears:

$$\sigma = \frac{1}{2} \left| \frac{2\pi}{\lambda} n_{eh} + \frac{i}{2} \sigma_{eh} \right|. \qquad (A3.4)$$

It has the dimension of a cross section and we use it to characterize the sample nonlinearity. In this case the diffraction efficiency is

$$\rho_s \sim \left[\left(\frac{2\pi n_{eh}}{\lambda} \right)^2 + \left(\frac{\sigma_{eh}}{2} \right)^2 \right] (N_1 l/2)^2 e^{-\alpha l} \qquad (A3.5a)$$

or

$$\rho_s \sim \left[\left(\frac{2\pi n_{eh}}{\lambda} \right)^2 + \left(\frac{\sigma_{eh}}{2} \right)^2 \right] (N_G l/2)^2 e^{-\alpha l} \qquad (A3.5b)$$

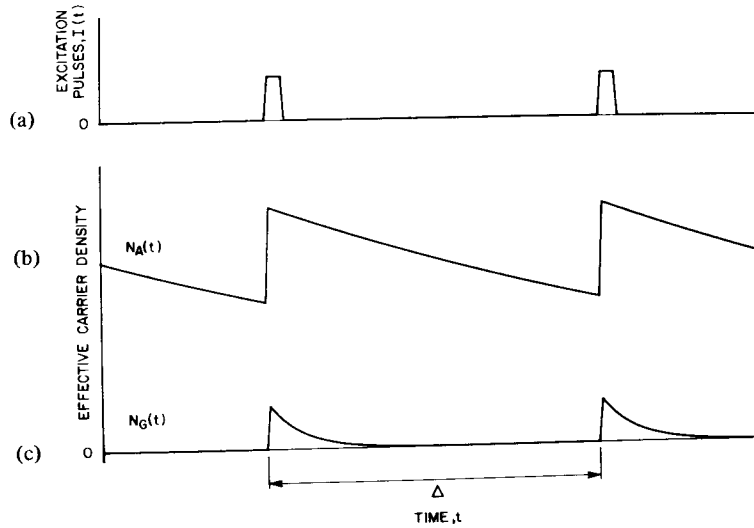respectively, for a short pulse and a CW excitation. On the

Fig. 11. For an excitation by a train of pulses $I(t)$, short compared to the lifetimes τ_A and τ_G and separated by a time Δ as shown on curve (a), the effective number of carriers for nonlinear absorption $N_A(t)$ and degenerate four-wave mixing $N_G(t)$ are shown on curves (b) and (c), respectively.

simple analytical expressions (A3.2) and (A3.5), corrections for Gaussian beam profile can be exactly accounted for [38].

The relation of this description to that in the frequency domain is straightforward for monochromatic waves. In the case where $I_p \gg I_t$ the solution of the coupled wave equation is [3]

$$I_s(l) = I_t(0) e^{-\alpha l} \frac{[\frac{1}{2} |\kappa| I_p l_\alpha]^2}{[1 + \alpha_2 I_p l_\alpha]^3} \qquad (A3.6a)$$

$$I_t(l) = I_t(0) \frac{e^{-\alpha l}}{[1 + \alpha_2 I_p l_\alpha]^2} + I_s(l) \qquad (A3.6b)$$

where the nonlinear coupling coefficient is

$$\kappa = \frac{32\pi^2 \omega}{n^2 c^2} \chi^{(3)}(-\omega; \omega, \omega, -\omega) = \frac{4\pi}{\lambda} n_2 + i\alpha_2.$$

In the small signal regime (A3.6) reduces to

$$\rho_t = (1 - 2\alpha_2 I_p l_\alpha) e^{-\alpha l} \qquad (A3.7a)$$

$$\rho_s = \left[\left(\frac{2\pi}{\lambda} n_2\right)^2 + \left(\frac{1}{2}\alpha_2\right)^2 \right] I_p^2 l_\alpha^2 l^{-\alpha l}. \qquad (A3.7b)$$

The two descriptions coincide if we consider that the effective number of carriers is $N_{\text{eff}} = (1/2)(\alpha\tau/\hbar\omega) I_p$ where $\tau = \tau_A$ or τ_G. Then

$$\alpha_2 I_p = \sigma_{eh} N_{\text{eff}}$$

$$n_2 I_p = n_{eh} N_{\text{eff}}.$$

The factor $1/2$ in the expression of N_{eff}, which originates from the development of the Bessel function, corresponds to the degeneracy factor 2 appearing in the frequency domain description, which accounts for the difference between self-effects (A3.7b), and induced effects [7] (A3.7a).

The description of mode-locked pulse interaction in the frequency domain is more elaborate. In this case, the fields are superpositions of modes of very close frequencies ω_m, the nonlinear susceptibility involved in this problem is $\chi^{(3)}(-\omega_l; \omega_m, \omega_{m'}, \omega_{m''})$, which contains terms of the form $[i(\omega_l - \omega_m) + \tau^{-1}]^{-1}$. Because the inverse of the carrier lifetime is small compared to the mode separation, only the pump and test

waves which originate from the same laser mode are effectively coupled. In the case $\tau^{-1} \gg (\omega_l - \omega_m)$, the average intensities also satisfy relations similar to (A5).

REFERENCES

[1] P. W. Smith, "On the physical limits of digital optical switching and logic elements," Bell Syst. Tech. J., vol. 61, pp. 1975–1993, 1982.

[2] For recent reviews see A. Miller, D.A.B. Miller, and S. D. Smith, "Dynamic nonlinear optical processes in semiconductors," Adv. Phys., vol. 30, pp. 697–800, 1980; see also D.A.B. Miller, "Dynamic nonlinear optics in semiconductors," Laser Focus, vol. 19, no. 7, pp. 61–68, 1983; see also R. K. Jain and M. B. Klein, "Degenerate four-wave mixing in semiconductors," in Phase Conjugation, R. A. Fisher, Ed. New York: Academic, 1983.

[3] D.A.B. Miller, D. S. Chemla, P. W. Smith, A. C. Gossard, and W. T. Tsang, "Room-temperature saturation characteristics of GaAs-GaAlAs multiple quantum well structures and of bulk GaAs," Appl. Phys., vol. B28, pp. 96–97, 1982.

[4] D.A.B. Miller, D. S. Chemla, D. J. Eilenberger, P. W. Smith, A. C. Gossard, and W. T. Tsang, "Large room-temperature optical nonlinearity in GaAs/Ga$_{1-x}$Al$_x$As multiple quantum well structures," Appl. Phys. Lett., vol. 41, pp. 679–681, 1982.

[5] D.A.B. Miller, D. S. Chemla, D. J. Eilenberger, P. W. Smith, A. C. Gossard, and W. Wiegmann, "Degenerate four wave mixing in room-temperature GaAs/GaAlAs multiple quantum well structures," Appl. Phys. Lett., vol. 42, pp. 925–927, 1983.

[6] D.A.B. Miller, D. S. Chemla, P. W. Smith, A. C. Gossard, and W. Wiegmann, "Nonlinear optics with a diode laser light source," Opt. Lett., vol. 8, pp. 477–479, 1983.

[7] See, for instance, D. S. Chemla and A. Maruani, "Nonlinear optical effects associated with excitionic-molecules in large gap semiconductors," Progr. Quantum Electron., vol. 8, pp. 1–77, 1982.

[8] A. C. Gossard, "Molecular beam epitaxy of superlattices in thin films," in Thin Films: Preparation and Properties, K. N. Tu and R. Rosenberg, Eds. New York: Academic, 1983, pp. 13–65.

[9] L. Esaki and R. Tsu "Superlattice and negative differential conductivity in semiconductors," IBM J. Res. Develop., vol. 14, pp. 61–65, 1970.

[10] R. Dingle, W. Wiegmann, and C. H. Henry, "Quantum states of confined carriers in very thin Al$_x$Ga$_{1-x}$As-GaAs-Al$_x$Ga$_{1-x}$As heterostructures," Phys. Rev. Lett., vol. 33, pp. 827–830, 1974.

[11] L. L. Chang, L. Esaki, and R. Tsu, "Resonant tunneling in semiconductor double barriers," Appl. Phys. Lett., vol. 24, pp. 593–595, 1974.

[12] R. Dingle, A. C. Gossard, and W. Wiegmann, "Direct evidence of superlattice formation in a semiconductor heterostructure," Phys. Rev. Lett., vol. 34, pp. 1327–1330, 1975.

[13] R. C. Miller, D. A. Kleinman, W. A. Nordland, and A. C. Gossard, "Luminescence studies of optically pumped quantum wells in

GaAs-Al$_x$Ga$_{1-x}$As multilayer structures," *Phys. Rev.*, vol. B22, pp. 863-871, 1980.

[14] C. Weisbuch, R. C. Miller, R. Dingle, and A. C. Gossard, "Intrinsic radiative recombination from quantum states in GaAs-Al$_x$Ga$_{1-x}$As multi-quantum well structures," *Solid State Commun.*, vol. 37, pp. 219-222, 1981.

[15] R. C. Miller, D. A. Kleinman, W. T. Tsang, and A. C. Gossard, "Observation of the excited level of excitons in GaAs quantum wells," *Phys. Rev.*, vol. B24, pp. 1134-1136, 1981.

[16] C. Weisbuch, R. Dingle, A. C. Gossard, and W. Wiegmann, "Optical characterization of interface disorder in GaAs-Ga$_{1-x}$Al$_x$As multi-quantum well structures," *Solid State Commun.*, vol. 30, pp. 709-712, 1981.

[17] J. Hegarty, M. D. Sturge, A. C. Gossard, and W. Wiegmann, "Resonant degenerate four-wave mixing in GaAs multiquantum well structures," *Appl. Phys. Lett.*, vol. 40, pp. 132-134, 1982.

[18] J. Hegarty, M. D. Sturge, C. Weisbuch, A. C. Gossard, and W. Wiegmann, "Resonant Rayleigh scattering from an inhomogeneously broadened transition: A new probe of homogeneous linewidth," *Phys. Rev. Lett.*, vol. 49, pp. 930-932, 1982.

[19] C. V. Shank, R. L. Fork, B. I. Greene, C. Weisbuch, and A. C. Gossard "Picosecond dynamics of highly excited multiquantum well structures," *Surface Sci.*, vol. 113, pp. 108-111, 1982.

[20] T. Ishibashi, S. Tarucha, and H. Okamoto, "Exciton associated optical absorption spectra of AlAs/GaAs superlattices at 300K," in *Proc. Int. Symp. GaAs Related Compounds, Inst. Phys. Conf. Ser. No. 63*, Japan, 1981, pp. 587-588; see also S. W. Kirchoefer, N. Holonyak, K. Hess, D. A. Gulino, H. G. Drickamer, J. J. Coleman, and P. D. Dapkus, "Absorption measurements at high pressure on AlAs-Al$_x$Ga$_{1-x}$As-GaAs superlattices," *Appl. Phys. Lett.*, vol. 40, pp. 821-824, 1982.

[21] H. M. Gibbs, S. S. Tarng, J. L. Jewell, D. A. Weinberger, K. Tai, A. C. Gossard, S. L. McCall, A. Passner, and W. Wiegmann, "Room-temperature excitonic optical bistability in a GaAs-GaAlAs superlattice etalon," *Appl. Phys. Lett.*, vol. 41, pp. 221-222, 1982.

[22] D. S. Chemla, "Quasi-two-dimensional excitons in GaAs/Al$_x$-Ga$_{1-x}$As semiconductor multiple quantum well structures," *Helv. Phys. Acta*, vol. 56, pp. 607-637, 1983.

[23] A. Baldereschi and N. C. Lipari, "Energy levels of direct excitons in semiconductors with degenerate bands," *Phys. Rev.*, vol. B3, pp. 439-451, 1971.

[24] M. Shinada and S. Sugano, "Interband optical transitions in extremely anisotropic semiconductors, I. Bound and unbound exciton absorption," *J. Phys. Soc. Japan*, vol. 21, pp. 1936-1946, 1966.

[25] R. L. Greene and K. K. Bajaj "Binding energies of Wannier excitons in GaAs-Ga$_{1-x}$Al$_x$As quantum well structures," *Solid State Commun.* vol. 45, pp. 831-835, 1983.

[26] C. Weisbuch, R. Dingle, A. C. Gossard, and W. Wiegmann, "Optical characterization of interface disorder in multiquantum well GaAs-Al$_x$Ga$_{1-x}$As superlattice structures," *J. Vac. Sci. Technol.*, vol. 17, pp. 1128-1129, 1980.

[27] V. I. Alperovich, V. M. Zalekin, A. F. Kranchenko, and A. S. Terekhev, "The influence of phonons and impurities on the broadening of excitonic spectra in gallium arsenide," *Phys. Status Solidi*, vol. B77, pp. 466-471, 1976.

[28] J. S. Blakemore, "Semiconducting and other major properties of gallium arsenide," *J. Appl. Phys.*, vol. 53, pp. R123-R181, 1982.

[29] F. Stern, "Elementary theory of the optical properties of solids," in *Solid State Physics*, vol. 15, F. Seitz and D. Turnbull, Eds. New York: Academic, 1963, pp. 299-408.

[30] ——, "Polarizability of a two-dimensional electron gas," *Phys. Rev. Lett.*, vol. 18, pp. 540-548, 1967.

[31] F. Stern and W. E. Howard, "Properties of semiconductor surface inversion layers in the electric quantum limit," *Phys. Rev.*, vol. 163, pp. 816-835, 1967.

[32] T. Ando, A. B. Fowler, and F. Stern, "Electronic properties of two-dimensional systems," *Rev. Mod. Phys.*, vol. 54, pp. 437-672, 1982.

[33] P. B. Visscher and L. M. Falicov, "Dielectric screening in a layered electron gas," *Phys. Rev.*, vol. B3, pp. 2541-2547, 1971.

[34] A. L. Fetter, "Electrodynamics of a layered electron gas II periodic array," *Ann. Phys.*, vol. 88, pp. 1-25, 1974.

[35] D. E. Aspnes, S. M. Kelso, C. G. Olson, and D. W. Lynch, "Direct determination of sizes of excitations from optical measurements on ion-implanted GaAs," *Phys. Rev. Lett.*, vol. 48, pp. 1863-1866, 1982.

[36] H. J. Eichler and F. Massman, "Diffraction efficiency and decay times of free-carrier gratings in silicon," *J. Appl. Phys.*, vol. 53, pp. 3237-3242, 1982.

[37] P. Kolodner, H. S. Kwok, J. G. Black, and E. Yablonovitch, "Exact decomposition of a Gaussian-averaged nonlinear function," *Opt. Lett.*, vol. 4, pp. 38-39, 1979.

Daniel S. Chemla was born in Tunis, Tunisia, on July 21, 1940. He graduated from L'Ecole Nationale Superieure des Telecommunications, Paris, in 1965. He received the Doctorat Es-Sciences from the Faculty of Sciences of Paris in 1972.

From 1965 to 1967 he worked at Le College de France in high-energy physics. From 1967 to 1981 he worked at the Centre National d'Etudes des Telecommunications as an MTS, Group Leader, and Department Head. He joined Bell Laboratories, Holmdel, NJ, in 1981 and is presently the Head of the Quantum Physics and Electronic Research Department. He has been engaged in research on nonlinear optics of insulators, organic molecules and crystals, and semiconductors. He is currently interested in the optical response of microstructures under excitation by ultrashort and high-intensity light pulses.

*

David A. B. Miller was born in Hamilton, U.K., in 1954. He received the B.Sc. degree in physics from the University of St. Andrews, St. Andrews, Scotland, in 1976 and the Ph.D. degree from Heriot-Watt University, Edinburgh, Scotland, in 1979.

He remained at Heriot-Watt University until 1981, latterly as a Lecturer in the Department of Physics, before moving to Bell Laboratories, Holmdel, NJ, where he is currently a member of the Technical Staff in the Department of Laser Science Research. His research interests include low-power nonlinear optical effects in semiconductors and optical bistability.

*

Peter W. Smith (M'67-SM'76-F'78), for a photograph and biography, see p. 36 of the January 1984 issue of this JOURNAL.

*
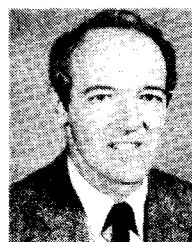
Arthur C. Gossard was born in Ottawa, IL, in 1935. He received the B.A. degree in physics from Harvard University, Cambridge, MA, in 1965 and the Ph.D. degree in physics from the University of California, Berkeley, in 1960.

He came to Bell Laboratories in 1960 and did research on nuclear and electron magnetic resonance in metals and magnetic materials. In 1974, he started work on molecular beam epitaxy, concentrating on the synthesis of very thin layers. He has published 180 papers and is presently a member of the Technical Staff in the Solid State Electronics Research Laboratory of Bell Laboratories, Murray Hill, NJ.

Dr. Gossard is a Fellow of the American Physical Society.

*

William Wiegmann was born in New York City in 1923.

He joined the Development Shops of Bell Laboratories in 1941 and shortly thereafter spent three years in the U.S. Air Force. After returning to Bell Laboratories he became involved in some of the early transistor and optoelectronic device development. For the past 13 years he has been involved in the MBE growth of GaAs and GaAlAs structures of all types as well as the engineering and fabrication of the MBE systems used in the growth process. He is presently a member of the Technical Staff in the Solid State Electronics Research Laboratory, Bell Laboratories, Murray Hill, NJ.